Metrol. Meas. Syst., Vol. XVIII (2011), No. 4, pp. 607-620.

PAN POLSKA AKADEMIA NAUK

METROLOGY AND MEASUREMENT SYSTEMS

Index 330930, ISSN 0860-8229

www.metrology.pg.gda.pl

M&MS

INFRARED IMAGING FOURIER TRANSFORM SPECTROMETER AS THE STAND-OFF GAS DETECTION SYSTEM

Mariusz Kastek, Tadeusz Piątkowski, Piotr Trzaskawka

Military University of Technology, Institute of Optoelectronics, gen. Sylwestra Kaliskiego 2, 00-908 Warsaw, Poland
(✉mkastek@wat.edu.pl, +48 22 68 39 383*)*

Abstract

The article presents the detection of gases using an infrared imaging Fourier-transform spectrometer (IFTS). The Telops company has developed the IFTS instrument *HyperCam*, which is offered as a short- or long-wave infrared device. The principle of *HyperCam* operation and methodology of gas detection has been shown in the paper, as well as theoretical evaluation of gas detection possibility. Calculations of the optical path between the IFTS device, cloud of gases and background have been also discussed. The variation of a signal reaching the IFTS caused by the presence of a gas has been calculated and compared with the reference signal obtained without the presence of a gas in IFTS's field of view. Verification of the theoretical result has been made by laboratory measurements. Some results of the detection of various types of gases has been also included in the paper.

Keywords: gas detection, hyperspectral detection, imaging Fourier-transform spectrometer, stand-off detection.

1. Introduction

The problem of remote detection of chemical substances appears in many, sometimes extremely different fields of human activities. Applications of detection devices include monitoring of technological processes, diagnostics of industrial installations, monitoring of the natural environment and military purposes. Such diversity has caused the development of many detection methods employing various physical phenomena due to which detection and identification of chemical compounds are possible. Among these methods, a significant group constitutes the solutions using the phenomenon of selective absorption of electromagnetic radiation by a chemical compound. Here, we can distinguish the solutions based on absorption of laser radiation emitted by an illuminator, being an element of a measuring system, and thermovision methods recording thermal radiation. The methods of the first group are the active methods employing absorption of laser radiation by chemical compounds. Thermovision methods are using the absorption bands of chemical compounds in an IR spectrum.

Thermovision methods, employing detector arrays, provide an image (in real time) of the observed scenery with marked regions of occurrence of the searched chemical substances. The usefulness of this method results from the fact that a lot of substances and chemical compounds have their absorption bands in the IR spectral range. Fig. 1 shows absorption bands of selected chemical compounds.

The devices operating in IR band, used for the detection of chemical substances (gases) in the atmosphere have their spectral characteristics and resolution matched to the absorption bands of compounds to be detected. Two types of such devices can be distinguished. The first one is a system similar to a typical thermal camera but additionally equipped with a filter

Article history: received on June 15, 2011; received in revised form on Sept. 8, 2011; accepted on Nov. 18, 2011; available online on Dec. 12, 2011.

system ensuring the required spectral resolution and a signal analysis system. The other type includes the device based on the principles of Fourier spectroscopy (Fourier Transform Infrared Spectroscopy - FTIR).

Fourier-transform spectrometers are renowned instruments, particularly well-suited to remotely provide excellent estimates of quantitative data. Many authors have presented how the conventional (non-imaging) FTS could be used to perform a quantification of distant gas emissions. Amongst others, we should mention the important contributions made by Harig [1, 2]. His group performed many measurement campaigns with excellent results, mainly by ensuring proper modelling of the scene and by taking into account the signature of the instrument used. Other groups developed similar approaches, however limiting their study to optically thin plumes [3, 4], to dedicated instruments performing optical subtraction [5, 6], or introducing Bayesian algorithms to maximize the use of *a priori* information [7]. On the other hand, detection and quantification activities with an imaging Fourier-transform spectrometer (IFTS) have been first presented in [8].

The present paper deals with remote gas identification and quantification from turbulent stack plumes with an IFTS method. It presents first the modelling that is required in order to get an appropriate understanding of both the scene and the instrument. Next it covers the methodology of the developed quantification approach. Finally, results are presented to demonstrate the capabilities and the performances of the remote gas quantification by using hyperspectral data obtained from the Telops *HyperCam* spectrometer. The latter is described in much detail in the references [9-12].

2. Instrumentation

The infrared imaging Fourier-transform spectrometer (IFTS) – *HyperCam* – used during the experiment was built by Telops, Inc. This IFTS has 320x256 pixel Mercury Cadmium Telluride (MCT) focal plane arrays (FPAs) with a 6º x 5º FOV. The FPAs are Sterling cooled to provide good noise figures in a field-ready package. Spectral information is obtained using a technique called Fourier Transform Infrared Radiometry (FTIR). FTIR is a classical interference based technique applied to gas spectroscopy that uses a Michelson interferometer to mix an incoming signal with itself with several different discrete time delays. The resulting time domain waveform, called an interferogram, is related to the power spectrum of the scene through the Fourier transform. An interferogram for each pixel in an image is created by imaging the output of the interferometer onto a focal plane array and collecting data at each discrete time delay. Advantages of using the FTIR sensor over a grating based (filter) system include higher resolution for equal cost and the absence of misalignment of different color images due to platform motion. However, FTIR does have the disadvantage of producing a slower frame rate than filter based systems because twice as many points are taken for the same number of spectral points. For an atmospheric tracking of gases however, the *HyperCam* sensor has a sufficient frame rate [8, 11].

Fig. 1. HyperCam sensor during the measurement.

The data can be collected with 0.25–150 cm^{-1} spectral resolution between 830 cm^{-1} (12 µm) and 1290 cm^{-1} (7.75 µm) at a frame rate of 0.2 Hz. In addition to the infrared data, a visible imagery can be recorded using the video camera boresighted to the IR sensor. Fig. 1 shows a picture of the *HyperCam* device during the measurement session. The sensor is controlled by a field computer and the recorded data is stored on a RAID drive to guarantee data integrity [12]. The *Reveal* software package is provided for the *HyperCam* control, registration and calibration of raw data, and for the data analysis as well. Fig. 2 presents the main window of *Reveal Pro* software used for controlling the parameters of the *HyperCam* device and visualization of the registered data. Fig. 3 shows the example of data analysis.

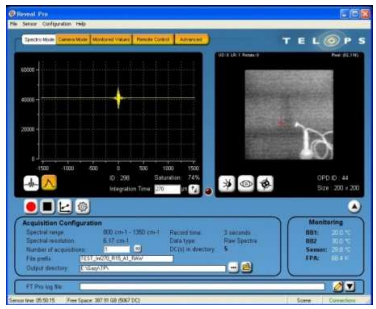

Fig. 2. Reveal Pro software for the control of *HyperCam* sensor.

a) b)

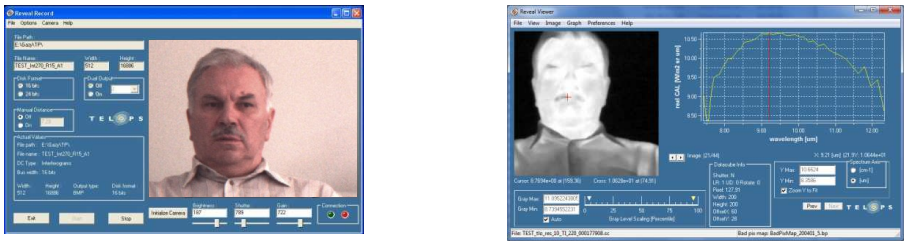

Fig. 3. Software for data analysis: (a) recorded visible image, (b) analysis of spectral data for marked point.

Imaging Fourier-transform spectroradiometer – *HyperCam* - uses the layout of a Michelson interferometer. Its schematic diagram, showing the elements responsible for the change of the length of optical path, is shown in Fig. 4.

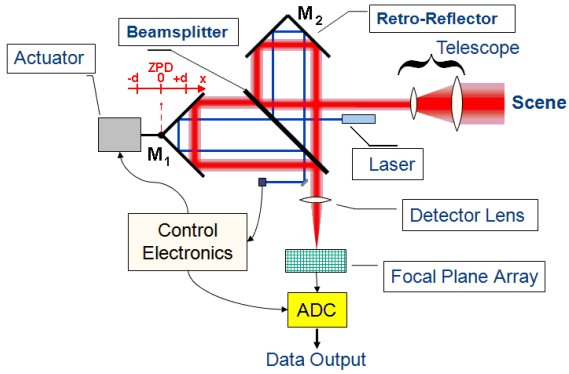

Fig. 4. Block diagram of imaging Fourier-transform spectroradiometer.

In the presented system the retro-reflectors are used instead of flat mirrors. As a result it is easier to move the M_1 mirror keeping the reflecting plane in constant position with respect to the optical axis. It should be mentioned here that the interferometer works in the far infrared range, thus the necessary difference in optical paths requires large mirror travel. For such long moves in a classical setup with flat mirrors the skew of mirror plane is difficult to avoid which may result in considerable measurement errors. The solution presented in Fig. 4. minimizes such errors.

The main difference between the standard and imaging interferometer is the application of a focal plane array (FPA) detector type. The imaging device can be described as classical interferometer multiplied by the number of pixels in the array. As a result the spectral analysis of interferograms at single pixels gives the spectral information of the entire image. The analysis of incident radiation at pixel level is identical for every array element. The change in amplitude as a result of optical path difference (OPD) x, for λ_i wavelength is given by:

$$A(x) = A_i \cos\left(2\pi \frac{x}{\lambda_i}\right). \tag{1}$$

Detector response is proportional to the radiant intensity of incident radiation:

$$I(t) = I_i \cos^2\left(2\pi \frac{x}{\lambda_i}\right). \tag{2}$$

Considering the trigonometric relations for the cosine of double angle and by limiting the analysis to a variable component only, the radiant intensity as the function of optical path difference can be written as:

$$I(x) = I_i \cos\left(4\pi \frac{x}{\lambda_i}\right). \tag{3}$$

For the sources with continuous radiation characteristics in the range from λ_1 to λ_2 , whose spectral characteristics (3) is described by a function $S(\lambda)$, the radiant intensity can be described as:

$$I(x) = \int_{\lambda_1}^{\lambda_2} S(\lambda) \cos\left(4\pi \frac{x}{\lambda}\right) d\lambda. \tag{4}$$

A typical interferogram illustrates radiant intensity as the function of the translation of M_1 mirror. Maximum of the output signal is achieved for zero path difference (ZPD).
Spectral distribution for a given pixel detector can be recreated using inverse Fourier transform, by calculating the following integral:

$$S(\lambda) = \int_{-\infty}^{+\infty} I(x) \cos\left(4\pi \frac{x}{\lambda}\right) dx. \tag{5}$$

In practical applications the optical path difference is realized in the finite, symmetrical range $\pm d$, so the relation (5) assumes the following form:

$$S(\lambda) = \int_{-d}^{+d} I(x) \cos\left(4\pi \frac{x}{\lambda}\right) dx. \tag{6}$$

The spectral distribution for an entire image is obtained by performing the analysis according to (6) for every pixel of an FPA array. The results can be treated as 3-dimensional data (two image coordinates and a wavelength).

The device described above is an imaging Fourier-transform infrared spectrometer. Such devices have several advantages. One of the most important parameter of any spectrometer is the product of its resolution and transmission. This coefficient is smallest for prism-type spectrometers. Grating-type spectrometers have this coefficient larger by several percent, whereas Fourier-transform devices boast up to two orders of magnitude advantage. It is particularly important in the infrared range, where the radiant intensity levels are usually much lower compared with the visual range. The resolution of Fourier-transform spectrometers is comparable with their grating-type counterparts. Further improvement can be achieved by applying longer optical path differences and by increasing the number of measurement points. Unfortunately both methods lead to longer measurement times, which are still the shortest in case of Fourier-transform spectrometers than in any other type. The advantage of an imaging spectrometer over scanning ones is that for a given optical path difference the entire image is analyzed simultaneously. Another advantage of the devices using Michelson interferometer layout is a quite large field of view. The telescope placed in front of the interferometer (Fig. 4) is optional and it is used only for the analysis of an object having small angular dimensions.

Summing things up, there are three ways to obtain an imaging spectroradiometer: thermal camera and a set of optical filters, thermal camera with a tunable filter or the Fourier-transform device described above. A simple "camera plus filters" setup has the worst parameters of these three. It has fixed imaging windows defined by the number of filters (usually not more than eight). Its operation is slow because filters are mechanically inserted into the optical path, e.g. by a rotation of a filter wheel. However it is a simple and cost-effective solution which can be used when the application does not require high spectral resolution, as in the detection of previously-selected gases in the chosen absorption band.

The other two solutions are more evenly matched in terms of parameters. The devices with tunable filters use a Fabry-Perot tunable etalon (especially in the LWIR range, 6 - 12 μm). One disadvantage of a such setup is the need for parallel translation of one element with respect to another in the Fabry-Perot layout. This translation range must cover the entire spectral range of the device. Additionally the incident beam must be parallel, because in other case the bandwidth is broadened for skew rays (central wavelength depends on the incident angle). There is also a need for additional optical filters defining the spectral range, because the transmission of a Fabry-Perot etalon is periodical. This complicates the optical design of the device. Spectral resolution is a tradeoff between transmission and resolution. Comparing spectrometers with tunable filters with Fourier-transform ones it can be stated, that the former have lower resolution and require telecentric optics but exhibit higher data acquisition rate, especially for its lowest spectral resolution. In Fourier-transform spectrometers the resolution and data acquisition rate are inversely proportional, so for the low resolution the data can be collected at speeds comparable to devices with tunable filters. The significant disadvantage of Fourier-transform devices is a complicated data processing technique. In current solutions data are processed by a dedicated computer. As a result such devices are now used mainly for R&D applications. In this area the flexibility of parameter choice (spectral resolution, spatial resolution and integration time) is more important than speed. However, in case of devices with a limited range of possible application the processing speed approaches real-time.

The described devices are referred to as spectroradiometers, but sometimes the more general spectrometer term is used. In case of prism or grating-type spectrometers the functional fragment called monochromator can be distinguished. Such devices can be used as

sources of quasi-monochromatic radiation. This functionality cannot be achieved with Fourier-transform spectroradiometers.

3. Model of a detection process

The physical problem of interest in the present paper concerns imaging Fourier-transform spectrometers taking measurements from a ground-based platform. Nevertheless, the approach described herein directly applies, with some adjustments, to airborne-based measurements. In the typical setup the instrument is looking towards a stack releasing gases.

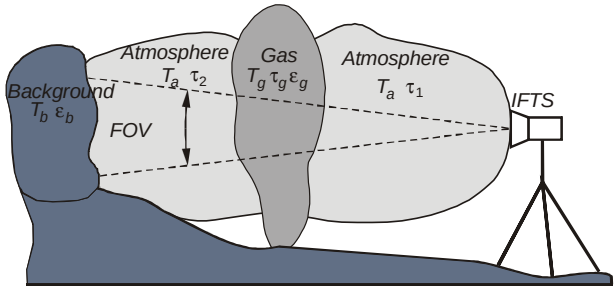

Fig. 5. Scheme of a measuring process and notations applied for the gas analysis in atmosphere.

The scene, from the instrument point-of-view, is implicitly inhomogeneous. Vertical variations of temperature and gas concentrations are necessarily present both in the released gases and in the atmospheric background. From the small instrument instantaneous field-of-view (FOV) – perspective, the instrument does see a small solid angle in a given direction, thus sensing a narrow pencil of an air mass. Within the illustrated disposition, any line of pixels therefore provides a complete section of the plume. Modelling the experimental conditions illustrated in Fig. 5 may be done by considering fundamentally two distinct aspects. The first deals with the whole contribution of the released gases through the atmosphere. And the second is devoted to understanding how the instrument itself does add its own signature into the measurement [11, 12].

In order to detect the gas plume, it is essential to begin with an underlying physics-based model for the hyperspectral data. This allows us to mathematically describe the radiance, defined as the flux per unit projected area per unit solid angle, incident at the sensor. This at-sensor radiance, $L(\lambda)$ is a summation of the contributions of numerous terms including both reflected solar and emitted thermal effects. In the LWIR band, emissive terms dominate and reflective effects are generally considered negligible [12].

For ground-based observation of a gaseous plume, the at-sensor radiance can be described as:

$$L(\lambda) = L_g(\lambda) + L_{b+g}(\lambda) + L_a(\lambda), \tag{7}$$

where: $L_g(\lambda)$ is the self-emitted radiance from the gas plume at wavelength λ, $L_{b+g}(\lambda)$ is the self-emitted radiance from the background transmitted through the plume, and $L_a(\lambda)$ is the scattered self-emitted atmospheric effects (also known as up welled radiance). The self-emitted radiance from the gaseous plume can be expanded such that:

$$L_g(\lambda) = \tau_1(\lambda)\varepsilon_g(\lambda)B(\lambda, T_g), \tag{8}$$

where: $\tau_1(\lambda)$ is the atmospheric transmittance from the gas plume to the sensor, $\varepsilon_g(\lambda)$ is the effective emissivity of the plume material, T_g is the temperature of the gas plume in Kelvin, and $B(\lambda, T_g)$ is Planck's blackbody curve given by:

$$B(\lambda, T_g) = \frac{2\pi hc^2 \lambda^3}{e^{\left(\frac{hc\lambda}{kT_g}\right)} - 1}, \tag{9}$$

where k is Boltzmann's constant, c is the speed of light, h is Planck's constant. Therefore the radiance seen at the sensor due to the gas plume is a function of the gas plume's emissivity, its temperature, and the atmosphere between it and the sensor. For the background, the radiance seen at the sensor is more complicated. This radiance is defined as:

$$L_{b+g}(\lambda) = \tau_1(\lambda)\tau_g(\lambda)\tau_2(\lambda)\varepsilon_b(\lambda)B(\lambda, T_b), \tag{10}$$

where: $\tau_g(\lambda)$ is the transmittance through the gas plume, $\tau_2(\lambda)$ is the atmospheric transmittance between the background and the gas plume, and $\varepsilon_b(\lambda)$ is the emissivity of the background material. In this case, the photons from the background travel through the atmosphere to the gas plume. The photons then travel through the gas plume which has its own transmittance function. The photons that make it through the gas plume travel the final distance to the sensor.

From equations (8), and (10), and using some simple algebra, the at-sensor radiance (7) can be rewritten such that:

$$L(\lambda) = \tau_1(\lambda)\left[\varepsilon_g(\lambda)B(\lambda, T_g) + \tau_2(\lambda)\tau_g(\lambda)\varepsilon_b(\lambda)B(\lambda, T_b)\right] + L_a(\lambda, T_a), \tag{11}$$

where T_a is the ambient air temperature.

To solve the (11), we have to know something about the atmospheric transmission, the temperature of the background, the temperature of the gas plume, the emissivity signature of the background, the scattering (or up welled radiance) term, and the emissivity signature of the plume.

Unfortunately, we only know the emissivity signature of the gas plume and the ambient air temperature; therefore, we must make some simplifying assumptions to use (11). The first assumption we make is that the atmospheric terms are negligible and/or are the same for all terms because all objects are relatively close to the camera. For the same reason, the second assumption we can make is that the up welled radiance term is also minimal and may be dropped. These assumptions lead to the following simplified model:

$$L(\lambda) \approx \varepsilon_g(\lambda)B(\lambda, T_g) + \tau_g(\lambda)\varepsilon_b(\lambda)B(\lambda, T_b), \tag{12}$$

The temperature at each pixel can be then calculated as:

$$T = \frac{hc\lambda}{k\log\left(\frac{2c^2\lambda^3}{L(\lambda)} + 1\right)}, \tag{13}$$

where: $L(\lambda)$ is the radiance signature for the pixel under test.

The background is the object for the sensor so left side of equation (12) can be expressed in terms of apparent emissivity and radiance of the background $B(\lambda, T_b)$. Using (12) and (13), an estimate for the temperature and Planck's blackbody curve can be created for every pixel in the scene. Each pixel can be divided by its estimated blackbody curve to obtain an estimate of its apparent emissivity:

$$\varepsilon(\lambda) = \varepsilon_g(\lambda)\frac{B(\lambda, T_g)}{B(\lambda, T_b)} + \tau_g(\lambda)\varepsilon_b(\lambda), \tag{14}$$

Another assumption we can make is that the factor multiplying plume emissivity can be roughly approximated as a function of the temperatures between the plume and the background:

$$\frac{B(\lambda,T_g)}{B(\lambda,T_b)} \approx f(T_g - T_b). \tag{15}$$

These assumptions of course could be removed and more robust atmospheric modeling and compensation implemented.

However, we have found that, for the relatively close stand-off distances considered (maximum distance ranges 150 m), the current simplified model yields good results. Thus using the assumption in (15), a new apparent emissivity model is described by:

$$\varepsilon(\lambda) = \varepsilon_g(\lambda) f(T_g - T_b) + \tau_g(\lambda)\varepsilon_b(\lambda). \tag{16}$$

Equation (8) suggests that the background can be modeled by only one emissivity; however, the background is typically comprised of multiple materials each with its own emissivity. In such a case, the apparent emissivity of the background is:

$$\varepsilon_b(\lambda) = \sum_{j=1}^{Q} \beta_j \varepsilon_j(\lambda), \tag{17}$$

where: Q is the number of unique background emissivity signatures, ε_j is the emittance for the j-th background signature and β_j is the amount of j-th background material. Using (17), the final apparent emissivity model is given by:

$$\varepsilon(\lambda) = \varepsilon_g(\lambda)\beta_0 + \tau_g(\lambda)\sum_{j=1}^{Q} \beta_j \varepsilon_j(\lambda), \tag{18}$$

where:

$$\beta_0 = f(T_g - T_b). \tag{19}$$

Therefore, each pixel in the scene is processed in the following manner. First, the apparent temperature is estimated using (13). From this estimate, the Planck's blackbody radiation curve is generated according to (9). The pixel value is divided by its blackbody radiation estimate to obtain (18). It is this equation can be used at the detection algorithm of gases. The algorithms of automation gases detection were under development and tests [10, 12]. The influence of emissivity coefficient on measurement results can also be compensated by adopting several methods from pyrometer non-contact temperature measurements. There are many known methods [13-16] for such compensation and an algorithm taking into account real emissivity values should be included in automatic gas detection procedures.

In the long wave infrared spectral range (LWIR), for chemicals in the gaseous form, scattering processes are not expected to contribute, so they are neglected. Note that this assumption would not be valid when aerosols are present. In general the spectral absorption coefficients may be dependent upon light polarization. However atmospheric absorption (and emission) being due to molecules, polarization dependence is not expected. Accordingly, the present description does not include polarization effects.

The absorption coefficient is made of a linear combination over the gas compounds of the atmosphere (linear mixture model). These coefficients are obtained from gas reference databases of infrared signatures (often in absolute absorbance values) as a function of the gas temperature (e.g. HITRAN molecular spectroscopic database [17] and Pacific Northwest National Laboratory (PNNL) Spectral Library [18]).

The transmission of the gas cloud τ_g is computed from the spectral properties of the chemical species using Beers' Law:

$$\tau_g(\lambda) = \exp\left(-\sum \alpha_i(\lambda) C_i d\right), \tag{20}$$

where: C_i is the average concentration of the chemical compound over the path length d and $\alpha_i(\lambda)$ is the wavelength-dependent absorption coefficient. The sum over index i in Eq. (20), is calculated over all spectrally relevant chemical species. PC MODWIN 3 v.1.0 computer program was used for the simulation of atmospheric transmission with the presence of a selected gas (e.g. methane) [19, 20].
The emissivity of a gas cloud is equal to its absorption which can be calculated from:

$$\varepsilon_g(\lambda) = 1 - \tau_g(\lambda), \tag{21}$$

On the basis of (20) and (21) the relation (16) can be written as:

$$\varepsilon(\lambda) = f(T_g - T_b) + \exp\left(-\sum \alpha_i(\lambda) C_i d\right)\left[1 - f(T_g - T_b)\right]. \tag{22}$$

The relation (22) indicates, that in case of IFTS measurement of gases in the open channel the effective emissivity depends on gas concentration C_i, attenuation coefficients α_i, cloud thickness in the direction of observation d and temperature difference between gas cloud and background $f(T_g\text{-}T_b)$. The aforementioned component related to temperature difference is calculated during the measurements. Contrary to the measurements in gas chamber the cloud thickness is unknown, so the measurement is affected by the product of gas cloud thickness and gas concentration. Additionally environmental conditions, such as wind speed, influence the measurement result because they cause variable gas concentrations at different distances from the measuring device.

IFTS technology can be used for the gas quantification but of course the methodology of this is now under the testing. This kind of algorithm uses some of filtering methods and methods for comparing the measurement results with the model ones [21]. Measurement sessions were performed in the laboratory and in the open-space conditions to practically verify the possibility of applying IFTS-type spectroradiometer for gas detection. The *HyperCam LWIR* device was used for the experiment and four different gases were observed. During the laboratory experiments the ambient temperature and humidity were monitored and during open-space tests the wind speed and direction and atmospheric pressure were additionally recorded.

4. Laboratory tests

The laboratory tests were performed in order to test the effectiveness of imaging Fourier-transform spectroradiometer as a tool for the measurement of spectral characteristics of a single gas or gas mixtures. The real photo of the laboratory test stand used during experiments is depicted in Fig. 6.

The measurements on a test stand presented in Fig. 6 were performed in order to determine the minimal gas concentration which can be detected by *HyperCam LWIR* spectroradiometer. The flow from gas cylinder was controlled by a precise gas pressure regulator and large-area blackbody was used to determine the value of thermal contrast between gas cloud and background. The applied blackbody has a radiative area of 11 x 11 inch and its temperature difference ΔT can be set with respect to ambient or temperature value measured by an external sensor. In our case this external sensor was placed at the output of gas nozzle thus the thermal contrast between gas cloud and background (blackbody area) could be precisely set.

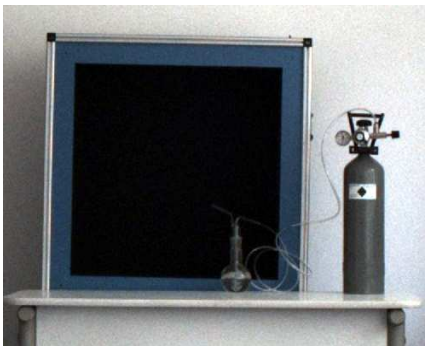

Fig. 6. The laboratory test stand.

The following gases were used during the measurements: NO_2, CO_2 and propane-butane mixture, all of those having absorption lines in the far infrared spectral range. Theoretical absorption spectra for CO_2 and NO_2 gases calculated by HITRAN software are presented in Fig. 7. Those characteristics were calculated for the same environmental conditions as recorded during laboratory tests, i.e. ambient temperature 294.2 K, and using Middle Lattitude Summer atmosphere model from commonly available database of atmospheric data from Modtran software. It can be seen from Fig. 7 plots that calculated spectra fit well inside the measurement range of *HyperCam LWIR* spectroradiometer and it can be expected that both gases should be detectable using this device.

a) b)

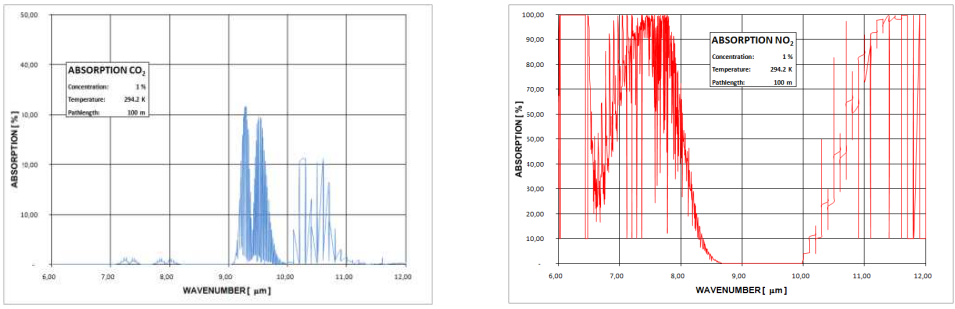

Fig. 7. The absorption of selected gases: (a) CO_2 (concentration 1%), (b) NO_2 (concentration 1%).

The applied gas pressure regulator provided the controlled gas flow. During the measurement session the flow was set at 5 mg/s which correspond to gas concentration of 1% in the measurement zone observed by a *HyperCam LWIR*. Spectral characteristics of gases were measured for the following values of thermal contrast: ΔT= 1 K, ΔT= 2 K, ΔT=3 K. In order to obtain the best possible accuracy the spectral resolution was set at 0.75 cm^{-1} whereas the frame rate was 0.3 Hz and it resulted from the chosen resolution of sub-frame windowing (limited area of an array used during measurements which also reduced the field of view). Each measurement was repeated twice in order to avoid accidental errors. The results obtained from *HyperCam LWIR* spectroradiometer gave finally the spectral characteristics of selected gases for different measurement conditions. The experimental results showing the measured spectral characteristics of CO_2 and NO_2 for different thermal contrast are presented in Fig. 8.

a) b)

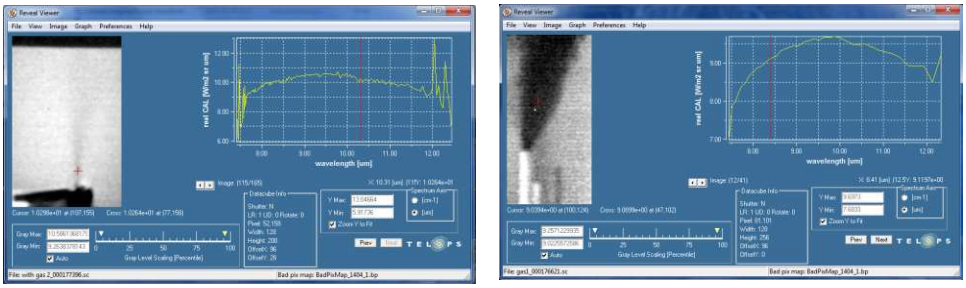

Fig. 8. The spectral results of gas measurements during laboratory tests: (a) CO_2 (concentration 1%, ΔT= 1 K), (b) NO_2 (concentration 1%, ΔT=3 K).

5. Field experiments

During the field tests the following gases were measured: CO_2, propane-butane mixture and freon 134 (CH_2FCF_3 tetrafluoroethane). In each case several gas concentrations were tested in order to verify the efficiency of gas measurements in the open space by *HyperCam LWIR*.

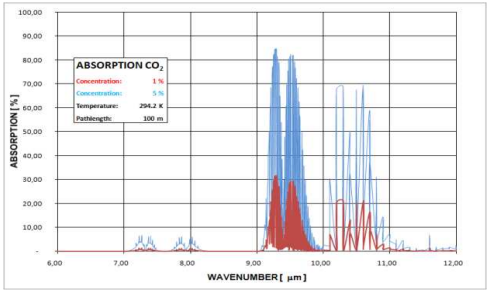

Fig. 9. The theoretical CO_2 absorption for two concentration values 1% and 5%.

Theoretical absorption spectra for two concentrations of CO_2 (1% and 5%) presented in Fig.9 were calculated using HITRAN software. As expected, higher gas concentration significantly increases the absorption and broadens its spectral range. During the experiment the absorption characteristics of CO_2 were also measured. The results of this measurement show the possibility to detect gases in the natural environments used the *HyperCam LWIR*. The measurement set-up with *HyperCam LWIR* spectroradiometer during field tests is shown in Fig. 10.

a) b)

Fig. 10. The measurement during field test at MUT area: (a) HyperCam spectroradiometer, (b) gas pipe and background plate.

Freon 134 was another gas used during the field measurements. This gas exhibits absorption bands in long wave infrared range, thus it can be detected using *HyperCam LWIR*. The registrations were made at two distances: 60 m and 10 m, for two gas concentrations of 3% and 6%. During the field measurements the weather conditions (humidity, pressure, wind speed and direction) were monitored by an automatic weather station Vantage Pro. It was observed that wind speed has the most significant influence on the measurement results. On the basis of the experience gained during the laboratory measurement sessions and previous measurements and theoretical analyses [19], it can be estimated that the thermal contrast ΔT (between gas cloud and background) above 3 K significantly increases the probability of gas detection by a *HyperCam* device. The results are presented in Fig. 11 and Fig. 12. The Matlab procedure applied for the analysis of data from *HyperCam* utilized the reference signature database and CMF module (Clutter Matched Filter). The reference signatures of gases were adopted from PNNL database. The algorithm used for gas detection is still under development and the presented results are preliminary. However, as it can be seen from Fig. 11b and Fig. 12b, the data processing by CMF module successfully reveals the presence of gas (marked by a red color).

a) b)

Fig. 12. The results of freon 134 measurements (concentration 3%, distance 60 m, T_{atm} = 18ºC, v_{wind} = 8 m/s , p_{atm} = 992 hPa): (a) spectral characteristics, (b) results of analysis in Matlab.

a) b)

Fig. 12. The results of freon 134 measurements (concentration 6%, distance 10 m, T_{atm} = 21ºC, v_{wind} = 1 m/s , p_{atm} = 998 hPa) : (a) spectral characteristics, (b) results of analysis in Matlab.

6. Conclusions

IFTS technique sensitivity is of order of magnitude lower than typical laboratory methods, mainly due to the fact that lock-in detection is not possible but the IFTS is a very useful method for gas detection in the open space. The possibility to present the results in a form of an image is a clear advantage, because the gas can be not only detected, but also located in space. Even its lower accuracy is still sufficient to detect and identify particular gases in the mixed gas cloud. On the basis of conducted experiments it can be stated that the gas

concentrations exceeding 2% can be detected in the open space using the *HyperCam* spectrometer.

The measurements conducted by means of IFTS spectrometers have lower accuracy due to lower sensitivity, the influence of weather conditions (mainly wind speed) and unknown thickness of a visualized gas cloud. Currently the new algorithm is under development, in which the cloud thickness will be automatically estimated on the basis of spatial distribution of areas with emissivity different than that of a background. This new method combining mathematical analysis, data from reference signature database (PNNL database), CMF (Clutter Matched Filter) module and additionally SAM (Spectral Angle Map) module should improve the effectiveness of gas detection by IFTS-based solutions.

References

[1] Harig, R., Matz, G. (2001). Toxic Cloud Imaging by Infrared Spectrometry: A Scanning FTIR System for Identification and Visualization. *Field Analytical Chemistry and Technology*, 5(1-2), 75-90.

[2] Harig, R., Matz, G., Rusch, P. (2002). Scanning Infrared Remote Sensing System for Identification, Visualization, and Quantification of Airborne Pollutants. *Proc. of SPIE*, 4574, 83-94.

[3] Griffin, M.K., Kerekes, J.P., Farrar, K.E., Burke, H.-H.K. (2001). Characterization of Gaseous Effluents from Modeling of LWIR Hyperspectral Measurements. *Proc. of SPIE*, 4381, 360-369.

[4] Burr, T., Hengartner, N. (2006). Overview of Physical Models and Statistical Approaches for Weak Gaseous Plume Detection using Passive Infrared Hyperspectral Imagery. *Sensors*, 6(12), 1721-1750.

[5] Lachance, R.L., Thériault, J.-M., Lafond, C., Villemaire, A.J. (1998). Gaseous emanation detection algorithm using a Fourier transform interferometer operating in differential mode. *Proc. of SPIE*, 3383, 124.

[6] Thériault, J.-M. (2001). Passive standoff detection of chemical vapors by differential FTIR radiometry, *Technical Report Defence Research Establishment Valcartier (DREV) TR-2000-156*.

[7] Heasler, P., Posse, C., Hylden, J., Anderson, K. (2007). Nonlinear Bayesian Algorithms for Gas Plume Detection and Estimation from Hyper-spectral Thermal Image Data. *Sensors*, 7, 905-920.

[8] Spisz, T.S., Murphy, P.K., Carter, C.C., Carr, A.K., Vallières, A., Chamberland, M. (2007). Field test results of standoff chemical detection using the FIRST. *Proc. of SPIE*, 6554, 655408.

[9] Farley, V., Chamberland, M., Lagueux, P., Vallières, A., Villemaire, A., Giroux, J. (2007). Chemical agent detection and identification with a hyperspectral imaging infrared sensor. *Proc. of SPIE*, 6661, 66610L.

[10] Vallières, A., Villemaire, A., Chamberland, M., Belhumeur, L., Farley, V., Giroux, J., Legault, J.-F. (2005). Algorithms for chemical detection, identification and quantification for thermal hyperspectral imagers. *Proc. of SPIE*, 5995, 59950G.

[11] Chamberland, M., Belzile, C., Farley, V., Legault, J.-F., Schwantes, K. (2004). Advancements in field-portable imaging radiometric spectrometer technology for chemical detection. *Proc. of SPIE*, 5416, 63-72.

[12] Farley, V., Belzile, C.; Chamberland, M., Legault, J.-F., Schwantes, K. (2004). Development and testing of a hyper-spectral imaging instrument for field spectroscopy. *Proc. of SPIE*, 5546, 29-36.

[13] Madura, H., Kastek, M., Piątkowski, T. (2007). Automatic compensation of emissivity in three-wavelength pyrometers. *Infrared Physics & Technology*, 51(1), 1-8.

[14] Madura, H., Kastek, M., Sosnowski, T., Orżanowski, T. (2010). Pyrometric method of temperature measurement with compensation for solar radiation. *Metrology and Measurement Systems*, 17(1), 77-86.

[15] Bielecki, Z., Chrzanowski, K., Matyszkiel, R., Piątkowski, T., Szulim, M. (1999). Infrared pyrometer for temperature measurement of objects of both wavelength- and time-dependent emissivity. *Optica Applicata*, 29(3), 284-292.

[16] Madura, H. , Piątkowski, T., Powiada, E. (2004). Multispectral precise pyrometer for measurement of seawater surface temperature. *Infrared Physics & Technology*, 46(1-2), 69-73.

[17] Champion, J.-P., Chance, K., Coudert, L.H., et al. (2009). The HITRAN 2008 molecular spectroscopic database. *Journal of Quantitative Spectroscopy and Radiative Transfer* 110, 533-572.

[18] Sharpe, S.W., Johnson, T.J., Sams, R.L., Chu, P.M., Rhoderick, G.C., Johnson, P.A. (2004). Gas-Phase Databases for Quantitative Infrared Spectroscopy. *Applied Spectroscopy,* 58(12), 1452-1461.

[19] Kastek, M., Sosnowski, T., Orżanowski, T., Kopczyński, K., Kwaśny, M. (2009). Multispectral gas detection method. *WIT Transactions on Ecology and the Environment*, 123, 227-236.

[20] Włodarski, M., Kopczyński, K., Kaliszewski, M., Kwaśny, M., Mularczyk-Oliwa, M., Kastek, M. (2009). Application of advanced optical methods for classification of air contaminants. *WIT Transactions on Ecology and the Environment,* 123, 237-247.

[21] Tremblay, P., Savary, S., Rolland, M., Villemaire, A., Chamberland, M., Farley, V., et al. (2010). Standoff gas identification and quantification from turbulent stack plumes with an imaging Fourier-transform spectrometer. *Proc. of SPIE*, 7673, 76730H.